IIETA International Information and Engineering Technology Association
Advancing the World of Information and Engineering

Traitement du Signal
Vol. 41, No. 6, December, 2024, pp. 3153-3162
Journal homepage: http://iieta.org/journals/ts

Active and Passive Antenna Sensor Signal for the Prediction of Breast Cancer Cell Size Below 3mm Using Bayesian Optimized Regression Analysis

Bindu Babu*, Sudha Suresh

Department of Electronics and Communication Engineering, Easwari Engineering College, Ramapuram 600089, India

Corresponding Author Email: bindu.tist@gmail.com

https://doi.org/10.18280/ts.410631

Received: 17 February 2024
Revised: 4 August 2024
Accepted: 6 November 2024
Available online: 31 December 2024

Keywords:
Antipodal Vivaldi Antenna (AVA), breast phantom, wavelet transform, microwave imaging, multiple tumor detection, SAR

ABSTRACT

Breast cancer between 2mm and 20mm is detected using mammogram images, with an accuracy of 85%. The accuracy percentage varies based on the density of tissues in the breast. Earlier detection of cancer cells, i.e., below 5mm size, increases the survival rate of breast cancer patients. This article proposes the use of a Tree-slotted Antipodal Vivaldi Antenna (TAVA) as a sensor to detect breast cancer cells in the 3mm to 5mm range through both passive and active sensing methods. TAVA antenna signals are acquired after inducing heat radiation over the breast region. Induced heating of cancer cells increases SAR and differentiates cancer cells of small size. TAVA active sensing signal-based SAR values are used for cancer detection. TAVA passive sensing signals are analysed with discrete wavelet transform, and statistical values are used for cancer cell detection. Moreover, Bayesian optimized regression is applied to statistical values obtained from active and passive sensing signals to predict the cancer cell size. Further, Breast Cancer Detection (BCD) devices such as Active Breast Cancer Device (ABCD) and Passive Breast Cancer Device (PBCD) are developed using TAVA antenna sensors such as active sensors and passive sensors, respectively. SAR analysis is performed through the proposed BCD device, detecting multiple tumors and predicting cancer cells with a size of less than 3mm. The accuracy of the proposed devices is about 99%.

1. INTRODUCTION

Breast cancer is the second leading disease among women and causes more deaths, according to the World Health Organization (WHO) reports 2021. Breast cancer-based death rates have increased in every part of the world. However, the death rate is higher among women in industrialized nations. In the current scenario, women with age less than 40 years compulsorily need to do Breast Cancer screening. For initial screening, physicians advise mammography or MRI imaging for the early detection of breast cancer. Breast cancer patients must undergo multiple screening techniques during the breast cancer cell diagnosis, which affects the patient's mental health.

MRI, PET, Ultrasound, and X-ray mammography are currently used for breast imaging. Minimal energy X-rays are used in X-ray mammography for breast cancer detection.

The above imaging modalities have certain limitations, such as exposure to ionizing radiation. Mammography shows 1/10th of the cases as false positives. X-ray mammography needs breast compression during the test, which causes severe discomfort. There is difficulty in detecting cancer cells in dense breast tissues. Moreover, frequent exposure to radiation at a young age causes tumours at a later age.

Ultrasound imaging has been reported as a painless method for detecting cancer cells at early stages compared to mammography. The resolution of ultrasound images is shallow, whereas MRI provides high-resolution images. A contrast liquid called gadolinium is injected during MRI scanning for a more explicit image. The adverse drug effect of gadolinium needs to be taken care of. MRI imaging is expensive and time-consuming. It will take 20-90 minutes to complete the procedure. MRI can never be used in pregnant women and patients with heart implants for breast cancer diagnosis [1].

Researchers are focusing on the development of an alternative imaging technique for breast cancer detection, which should be safe for women and solve the above limitations [2].

To solve the above drawbacks, scientists are focusing on microwave imaging. Microwave imaging differentiates the normal and cancerous tissue based on dielectric characteristics. Microwave imaging method never needs breast compression, ionization radiation, or contrast material. High-resolution 3D images are obtained using microwave imaging (MWI). MWI emits microwave radiation below the SAR limit of about 0.08 W/kg. The antennas used for microwave breast imaging must be in ultra-wide bands, which radiate in the range of frequencies with considerable gain and directivity [3]. The antenna must be small and fit around the breast region. Microwave imaging identifies minute signal fluctuations caused by cancer tissues. In Microwave Imaging, the breast tissue is exposed to microwave radiation. The breast tissue absorbs microwave energy while some energy is reflected. The dispersed microwave energy signals are recorded and processed for cancer detection. The features extracted from the microwave signal show the presence of the cancer [4].

Contributions: This paper uses a novel TAVA for the detection of cancer cells smaller than 3 mm in the intercoastal muscle region, lobules, nipple region, and the subcutaneous fat region of the breast phantom using active and passive TAVA as sensor. The above regions are dense breast tissues. The 3 mm cancer cell is detected by analyzing the S11 parameter and SAR values obtained from proposed ABCD devices and passive signal-based measurements in PBCD devices. Finally, Bayesian optimized multiple linear regression is applied to predict the size of the cancer cell. Multiple linear regression (MLR) effectively predicts the size of breast cancer cells, based on multiple features. Bayesian optimization of regression analysis enhances the performance by effective hyperparameter tuning, leading to accurate cancer cell size prediction. The main contributions of the proposed work are:

1. To detect the cancer cells of size below 3 mm located in the different dense regions of the breast, such as the intercoastal muscle region, lobules, nipple region, and the subcutaneous fat region of the breast phantom using active and passive TAVA as sensors.

2. To enhance cancer detection performance, external heat is applied to the breast region. The passive TAVA signals are analyzed with DWT, and statistical data for breast cancer detection are acquired.

3. To develop the ABCD device and PBCD device using TAVA as a sensor, Bayesian optimized linear regression (BO-LR), and Bayesian optimized multiple linear regression for breast cancer cell detection and prediction.

4. To compare the performance of the proposed devices (i) ABCD and (ii) PBCD using ground truth verification.

2. LITERATURE REVIEW

Researchers have designed different antennas such as microstrip patch antennas, Vivaldi antennas, monopole antennas, bowtie antennas, fractal, and horn antennas for various purposes such as sensors, rectenna and radiation.

Bhargava et al. [4] designed a 30 × 25 × 0.794 mm^3 sized microstrip patch antenna, and Confocal Microwave Imaging algorithm was used for the visualization of the image. The device detects the tumour, when the distance between the antenna is far away from the tumour. The patch antenna's operating bandwidth is less. Kaur and Kaur [5] designed a 3-layered Microstrip patch antenna with a '+' shaped defected ground structure with 37 × 43 × 4.85 mm^3 antenna size. The antenna gain is 6 dB at 9.1 GHz, and the radiation efficiency is 65%.

Palantei et al. [6] designed a microstrip patch antenna of size 24*22 mm^2. Two substrate materials such as FR-4 and NPC H220, are used. NPC H220 provides gain at the resonant frequency. Rajput et al. [7] designed a teeth-shaped rectangular microstrip applicator (TSRMA). TSRMA dimension is 36 × 24 ×1.55 mm^3. In TSRMA, FR-4 is used as a substrate. The designed antenna has a bandwidth of 912 MHz with a peak return loss of -22.95 dB at 2.68 GHz.

Dr. Gibson developed the Vivaldi antenna in 1979, which has a large bandwidth and consistent gain. Radar and 5G devices use Vivaldi antennas. In Vivaldi antennas, microstrip transmission feeder and antenna size determine the beamwidth and bandwidth. Vivaldi antenna has linear polarization, high gain, and wide operating bandwidth. Islam et al. [8] developed a metamaterial-based antenna with a high gain and size of about 46 × 40 × 1.57 mm^3. The substrate material used in the Vivaldi antenna is Rogers RT5880. To enhance the performance of the Vivaldi antenna, a metamaterial unit cell with negative permittivity is integrated into the back radiator opening layer. Although the design is compact, the antenna's feeding transition and geometric features are sensitive. Achieving a directional emission pattern and high gain using the Vivaldi antenna is challenging.

Islam et al. [9] developed a Vivaldi Antenna with dimensions of 88 × 75 × 1.57 mm^3 and used Rogers RT5870 as substrate material. Radiating fins in the antenna have etched six slots, extended the effective electrical length and leading to powerful directional radiation. It decreases the lowest working frequency range and increases gain and efficiency without reducing antenna size. The gain of the designed antenna is 9.8 dBi, and the average efficiency is 92%. Dr. Gazit discovered the Antipodal Vivaldi antenna (AVA) in 1988 to reduce beamwidth, side lobes, and return loss. The AVA had symmetrical design, with two identical flares positioned on opposite sides of the substrate. This arrangement reduces side lobes, return loss, and beamwidth, making the antenna's performance more efficient. The top flare is a conductor, while the bottom flare is the ground [10]. The designed antenna is a simplified design with improved performance.

Balaji et al. [11] designed a highly directional Ultra-Wide Band AVA with a 110× 98× 1.6 mm^3 dimension. The frequency range of the antenna is between 1.45 GHz and 9.8 GHz. Researchers [12] incorporate variations in the structure of the AVA, such as slotted AVA, which has an improvement of 73.65% compared with conventional AVA and exponential AVA with exponential dielectric lens [13]. Slot edges increase the lower operating frequency [14]. Herzi et al. [15] designed an AVA with the elliptical dielectric director and minimized the inter-components' mutual coupling.

Metamaterial (72 square shaped patch in multistep), Slots on the flare structure [16], and Elliptical director [17] in the antenna structure improve the gain and radiation pattern. A. M. de Oliveira et al. designed a Fern AVA antenna with a size of 150 × 150 × 1.6 mm^3 [18]. The antenna's performance is improved through oval slot edges at regular intervals. The AVA with dual radiating arms is positioned symmetrically on the substrate, with a 180° phase difference in excitation, enhancing both gain and radiation pattern. AVA is constructed with a Taconic TLT substrate having a permittivity of 2.55. This antenna design includes extra strip arms to improve the lower frequencies, reducing antenna size and enhancing return loss within the 2-5 GHz range. Additionally, the antenna provides an impedance frequency bandwidth of 185% [19]. A comparison of different antennas for biomedical applications is shown in Table 1. The proposed TAVA antenna has promising results regarding size, gain and bandwidth.

Table 1. Comparison of antennas

No.	Type of Antenna	Enhancement Technique Used	Dimension (mm) [L × W × H]	Substrate	Maximum Return Loss (dB)	Operating Frequency (GHz)	Application
[5]	MPA	Slots	37 × 43 × 4.85 (3 layered model)	FR-4	Lower than -35dB at 6 GHz	4.9-10.9	Early detection of breast cancer
[7]	MPA	Teeth shaped rectangular slots	36 × 24 × 1.55	FR-4	-25.6 at 2.76 GHz	2.368-3.28	Breast Hyperthermia
[9]	VA	Metamaterial	46 × 40 × 1.57	Rogers RT5880	Lower than -20dB at 9 GHz	2-10.45	Microwave Breast Imaging
[11]	AVA	Rectangular corrugations	98 × 110 × 1.6	FR-4	Lower than -20 dB near 2 GHz	1.45-9.8	Microwave Imaging and Radar applications
[12]	AVA	Slots	42.8 × 57.3 × 1.6	FR-4	Lower than -50 dB near 6 GHz	3.6-10	Microwave Imaging
[13]	AVA	Dielectric Lens	130 × 76 × 1	FR-4 Lens - Taconic CER-10	Lower than -35 dB at 9.6GHz	3.1-14	High-resolution imaging applications
[14]	AVA	Slots and Dielectric Lens	66.4 × 50 × 1	Not Mentioned ($\varepsilon_r = 4.5$)	Lower than -40dB between 10-15 GHz	4-30	High dynamic-range imaging radars
[15]	AVA	Rectangular slits, Directors, and Metamaterial	260 × 120 × 0.76	Not Mentioned ($\varepsilon_r = 3$)	Lower than −16 dB at 4.16–28 GHz	1-28	UWB application
[17]	AVA	High permittivity dielectric director	86 × 89.4 × 0.76	RF35 Director - Rogers R03010	Lower than -40 dB at 10 GHz	2.3-15	Radar applications and Satellite communications
[18]	AVA	Oval shaped slots	150 × 150 × 1.6	FR-4	-12.9 at 1.5 GHz	1.5-3.3	To detect brain tumor
[19]	AVA	Exponential Strip Arms	158 × 125 × 1	Taconic TLT	-35dB at between 14-16 GHz	0.72-17	UWB systems
[20]	AVA	Slots	90 × 80 × 1.524	ASTRA MT77 ($\varepsilon_r = 3$)	-31 dB at 7.368 GHz	1-13	UWD, Microwave Imaging, Radar
[21]	AVA	Rectangular gratings	45 × 24 × 1.28	Rogers 3010	-15.97dB at 4 GHz	0.6-5	Microwave Medical Imaging
Our Work	TAVA	Slots and Directors	53.07 × 46.07 × 0.6	FR-4	-36.2dB at 7.9GHz	1.6-13.8	Breast tumor Detection

Breast phantom

Researchers have developed real-time breast phantom models to detect the tumour in the breast. Rajput et al. [7] made two four-layered hemispherical Breast phantom models. In one model, an additional layer of water bolus is included. The four layers are used in the model such as Skin, Fat, Gland, and Muscle.

Islam et al. [22] developed a breast phantom with Polyethylene and agar, a homogenous or two-layered (skin and fat) phantom model. The agar-xanthium-based mixture is used for the four layers such as skin, fat, gland, and tumour. Materials such as distilled water, sodium dehydroacetate monohydrate, polyethene powder, xanthan gum, and agar powder are used to develop homogenous breast phantoms. Polyethylene powder changes permittivity, while NaCl improves the conductivity.

The phantom is kept in shape using agar. Sodium dehydroacetate monohydrate is used as a preservative which stops the water content separation, and xanthan gum is used as a thickener. Gelatin mixtures have dielectric properties in breast tissues and are stable for up to 8 weeks [22].

Studies have explored the usage of machine learning techniques, including regression, for detecting and diagnosing breast cancer.

Logistic regression, a type of regression analysis, has been used in some studies to improve breast cancer prediction accuracy and discriminate between benign and malignant breast disease.

The reflected signals from the breast phantom are analyzed by Patel and Raina [23] with Random Forest classifiers and detected the tumour with an accuracy of 83% [24], and classification using an SVM polynomial gives 88% accuracy for 100 training samples [25].

Inference from Literature Survey:

In most of the works, simulations are done in the homogenous phantom. There is difficulty in detecting cancer cells present in the heterogeneously dense fibro-glandular tissues. Most research works are carried out to detect cancer cell sizes greater than 5 mm. The proposed system can detect multiple tumors of size less than 3 mm.

3. PROPOSED WORK

This paper uses a compact-sized TAVA as the sensor. The efficient design of the antenna can easily identify the minute signal variations caused by the cancer cells. For the proposed study, a heterogenous breast phantom is created, mimicking the dielectric characteristics of the woman's breast. The breast phantom is heated with the heating pad. The heating pad increases the cancer cell temperature, improving the SAR and differentiating the smaller cancer cells from normal cells. In this study, ABCD and PBCD devices were developed based on active sensing and passive sensing.

The heating pad in the experimental setup temporarily raises the surface temperature of the breast tissue, allowing for more accurate readings. The periodic temperature fluctuations significantly improve the precision of the methods mentioned earlier. Researchers can create a phase map showing the relationship between the thermal stimulation and the breast surface's temperature response by thermally stimulating the tissue at a specific rate and simultaneously recording the signals with a TAVA antenna. The signal's amplitude is directly related to the heat dissipated at the surface. This induced heating enables the detection of minimal temperature differences, even when obscured by background noise.

The high sensitivity of the radiation reduces the signal strength in regular tissue areas, while large temperature gradients affect the breast tissue's thermal properties, such as blood flow. Furthermore, if the thermal modulation frequency is high, the TAVA antenna signal can be used to identify small breast cancer cells emitting a signal.

The proposed TAVA antenna is connected to a microwave radar sensor in active sensing that transmits microwave signals at 10 GHz. TAVA antenna is placed on breast phantom with cancer cells. The TAVA antenna transmits signal at the resonant frequency to the breast phantom. The reflected signals from the cancer cells are analyzed for the Specific Absorption Rate (SAR). It has been observed that cancer cells have the highest SAR value.

In passive sensing, the signals radiated from cancer cells, without transmitting signals, are processed using the MATLAB acquisition toolbox software, and the signal is analyzed through the discrete wavelet transform. The size of the tumour is predicted using the extracted features from DWT and the machine learning algorithm. Based on the active sensing of the TAVA antenna, the ABCD device is developed, and based on the passive sensing of the TAVA antenna, the PBCD device is developed. Figure 1 shows the block diagram of the proposed system.

The proposed study consists of five main sections. Section 1 delves into the discussion of the Proposed TAVA design, while Section 2 elaborates on the design of the breast phantom model. The SAR analysis using CST simulation is discussed for different locations of cancer cells in the breast phantom model in Section 3. Experimental analysis of tumour detection, i.e., both ABCD and PBCD device measurements, is elaborated in section 4. Section 5 explains cancer cell size prediction using a machine learning algorithm.

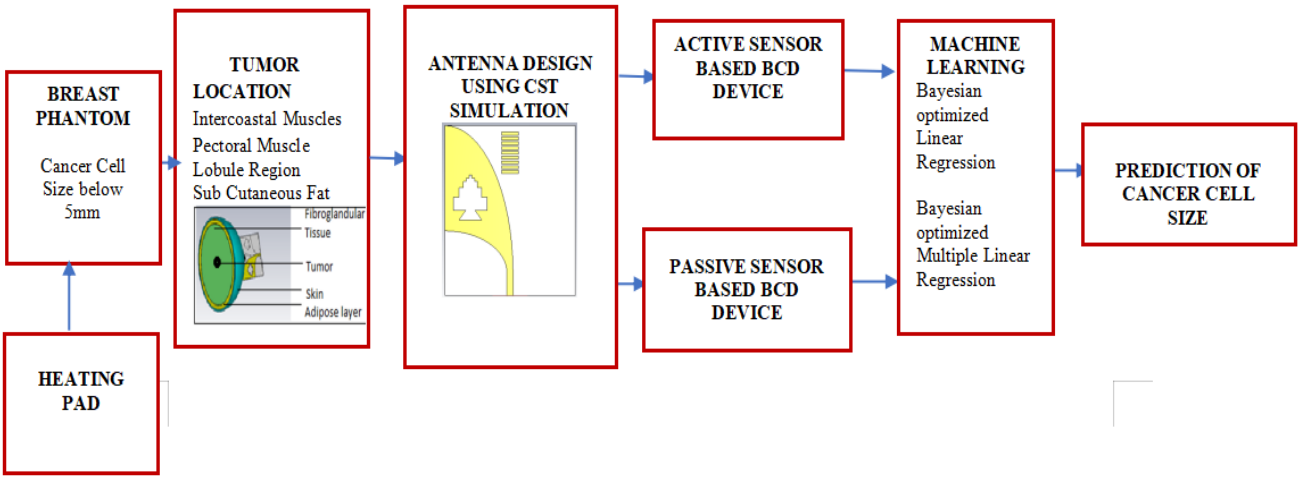

Figure 1. Block diagram of the proposed system

3.1 Proposed TAVA design

The TAVA design spans a frequency range of 1.63 GHz to 13.8 GHz. TAVA is fabricated with FR-4 as the substrate with a relative permittivity of 4.3 and a thickness of 0.6 mm. The substrate [8] features low permittivity and tangent loss to minimize power loss in the antenna. The antenna length (L) is determined by combining major radii of ellipse1 (r_{s1}) and the feeder height.

The substrate thickness (h) is also a key parameter. The Input Impedance of the antenna (Zo) is set at 50 Ω. Table 2 shows the details on the antenna specifications.

The TAVA antenna is shown in Figure 2, which consists of slots and directors. The dimensions of the TAVA are 53.07 × 46.07 × 0.6 mm^3. The exponential arms of the antenna are made of copper, and the thickness is about 0.036 mm - a tree-shaped slot increases stepwise on the front and back sides of the antenna. Directors in the rectangle are used in the AVA's front side, enhance metrics such as Return loss, Gain, and Directivity.

The detailed dimensions of the front and back views of the proposed AVA are illustrated in Figure 2.

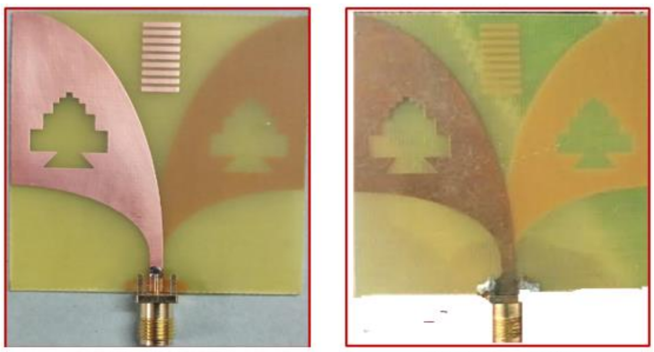

(a) Front view (b) Back view

Figure 2. Proposed TAVA design

Table 2. Proposed TAVA antenna parameters

Parameter	Dimension (in mm)	Description
W	46.7	width of antenna
L	53.7	length of antenna
H	0.6	substrate thickness
w_m	2.15	microstrip transmission feeder width
l_m	7	microstrip transmission feeder length
r_1	24.11	minor radii of ellipse 1
r_2	21.96	minor Radii of ellipse 2
rs_1	46.07	major Radii of ellipse 1
rs_2	13.176	major Radii of ellipse 2
w_d	6	director width
l_d	1	length of director
t_d	0.035	thickness of director
s_d	0.5	spacing between 2 directors

3.2 Design of breast phantom model

For this study, the developed breast phantom model, which consists of four layers, is used and is illustrated in Figure 3. The layers include skin layer, adipose Layer, fibro glandular layer, and a tumor. The skin layer has a radius of 50 mm, the adipose layer has a radius of 48 mm. Different sizes of cancer cells such as 3 mm, 4 mm, and 5 mm in radius are placed inside the phantom.

The various layers of the breast phantom model are created with dielectric properties which mimic the human breast [26] as shown in Table 3.

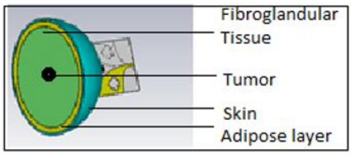

Figure 3. Breast phantom model design

Table 3. Dielectric properties of various layers of developed breast phantom model

Material	Epsilon	Electrical Conductivity (S/m)	Rho (Material Density) (kg/m^3)	Thermal Conductivity
Skin Layer	39.04	1.14	1109	0.37
Adipose Layer	5.287	0.0876	911	0.21
Fibro gland	58.08	1.52	1041	0.33
Tumor	54.9	4	1058	1.1

Breast Phantom with multiple tumors of size, such as 3 mm, 4 mm, and 5 mm, placed at the dense breast regions, such as the intercoastal muscle region, lobules, nipple region, and the subcutaneous fat region, as shown in Figure 4. The developed heterogeneous breast phantom model has three layers: the skin layer, the adipose layer, and the tumour.

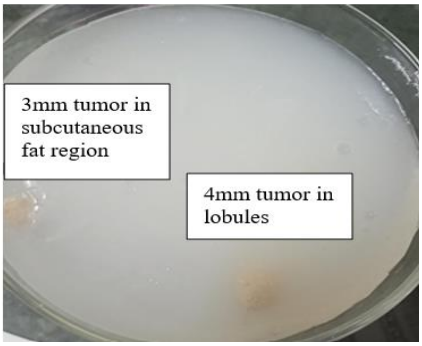

Figure 4. Real time breast phantom model with multiple tumor

3.3 SAR analysis using CST simulation

In this section, SAR analysis is measured using the CST software to identify the cancer cell location. The Specific Absorption Rate determines the electromagnetic field exposure in living tissues. SAR value varies based on tissue density, measured in kilograms per cubic meter, and its electrical conductivity is measured in Siemens per meter. The SAR level is influenced by the strength of the electric field generated by the radiated energy, measured in volts per meter. The SAR level for a tissue with a mass of 1 gram should not exceed 1.6 watts per kilogram. The SAR value decreases from the Skin Layer. Women aged 50 to 55 have breast layers with the highest SAR values.

The breast phantom model has 3 mm, 4 mm, and 5 mm cancer cells in various positions for experimentation. The designed phantom model has a depth of 40 mm. The breast phantom is kept near the antenna. The maximum SAR of 1.32 W/ Kg is obtained for a 4 mm cancer inserted in the position (0,0,25) in the phantom., as shown in Figure 5(a). In CST simulation, to view the field distribution, the model is cut along the YZ plane using a cutting plane. Similarly, a 5mm sized spherical cancer cell has maximum SAR value of 1.52 W/Kg, shown in Figure 5(b).

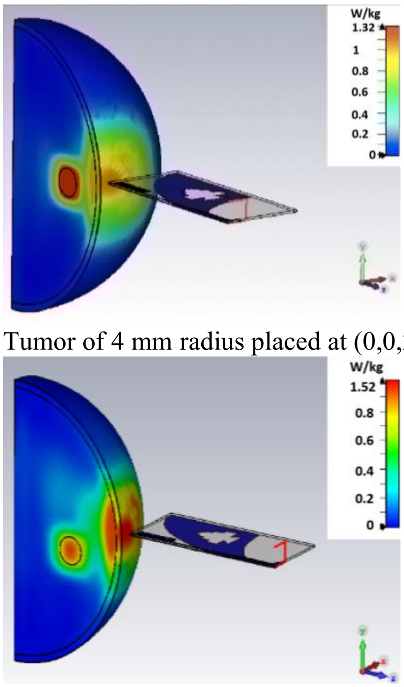

(a) Tumor of 4 mm radius placed at (0,0,25)

(b) Tumor of 5 mm radius placed at (3,-5,21)

Figure 5. Field distribution in SAR analysis of single tumor

The field radiation of SAR analyzed for multiple cancer cells is shown in Figure 6.

In CST, for experimental validation of multiple tumor identification, a 4 mm sized tumor is placed at (0.0,25) and a 5 mm sized tumor is placed at (3,-5,21). The two tumors listed are placed at various depths. The maximum SAR value is 0.27 W/Kg at (-0.26,-0.5,29.5).

Table 4 shows the detected cancer location for cancer sizes 3 mm, 4 mm and 5 mm using SAR values. Maximum radiation is obtained nearer to the cancer location.

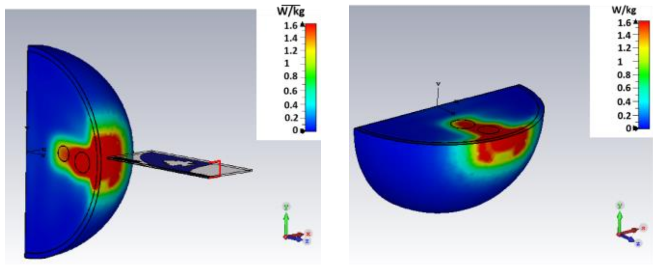

Figure 6. Field distribution of SAR analysis of multiple tumors, a 4 mm tumor placed at (0,0,30) and a 5 mm tumor placed at (-4,2,20)

Table 4. SAR analysis of 3 mm, 4 mm and 5 mm cancer cells using CST simulation

Actual Tumor Location	Detected Tumor Location					
	5 mm Tumor	Max SAR (W/Kg)	4 mm Tumor	Max SAR (W/Kg)	3 mm Tumor	Max SAR (W/Kg)
0,0,30	0.26,0.4,30.4	1.525	1.44,2,33.6	1.4	1.8,2.2,35.3	1.2
0,0,25	0.26,0.4,25.41	1.743	0.8,1.2,26.2	1.32	0.9,1.6,28.1	1.1
0,5,24	0.26,4.1,24.41	1.518	0.8,3.5,25.2	1.26	0.9,3.0,27.2	1.04
10,0,25	8.36,0.4,25.41	1.205	8.36,1.2,26.2	1.14	7.56,2.1,27.4	0.98
10,2,20	9.03,1.66,20.41	1.32	7.56,3.5,19.5	0.96	6.8,3.9,18.1	0.94
-5,2,25	-4,2.3,25	1.27	-3.33,2.9,26.2	0.99	-2.9,3.1,27.8	0.92
3,-5,21	3.33,-3.75,21.41	1.52	2.77,-3,22.2	1.01	2.2,-2.4,24.4	0.95
5,3,18	4.66,2.8,18.41	1.156	7.56,2.8,19.5	0.99	8.1,3.5,20.2	0.94

3.4 Proposed ABCD device for breast cancer detection

In active sensing, the antenna is connected to the VNA to transmit and receive the microwave signal. The directional antenna is kept in the direction of maximum radiation near the skin surface and measures backscattered signal S11 as in Figure 7.

The S11 value at resonant frequency without cancer cells is obtained as -25.91 dB and with cancer cells as -29.54 dB. The proposed ABCD devices replace the VNA with an HB100 microwave IC of 10.25 GHz for transmitting and receiving the signal. The received signal is connected to the microcontroller and is measured using node MCU. The block diagram of ABCD is shown in Figure 8(a), and the experimental setup is shown in Figure 8(b). Table 5 shows the S11 and SAR obtained for the cancer cells of sizes 3 mm, 4 mm, and 5 mm placed at the subcutaneous region. SAR value increases with the cancer size. Reflection is more for breast phantoms with cancer cells than without cancer cells because of the high moisture content in the tumor.

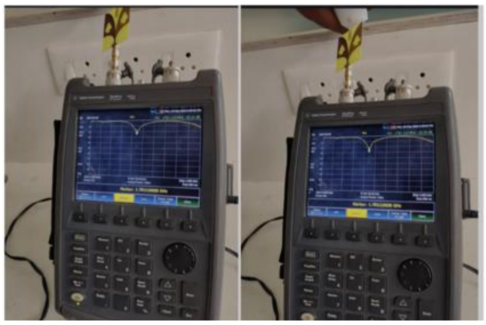

Figure 7. Measurement of S11 with and without tumor using VNA

Table 5. S11 and SAR values for cancer cells of sizes 3 mm/4 mm and 5 mm

Cancer Cell Size	Location of Cancer Cell in the Breast	S11 Values from VNA	Before Heat – SAR Values in W/Kg	After Heat- SAR Values in W/Kg
Without Tumor		-25.91dB	0.305	0.758
3mm	Subcutaneous region	-29.54dB	0.902	1.341
4mm	Subcutaneous region	-29.93 dB	1.232	1.543
5mm	Subcutaneous region	-30.23 dB	1.285	1.655

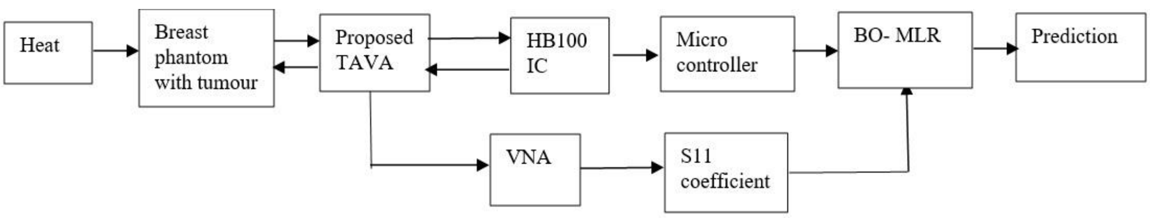

(a) Block diagram of ABCD device

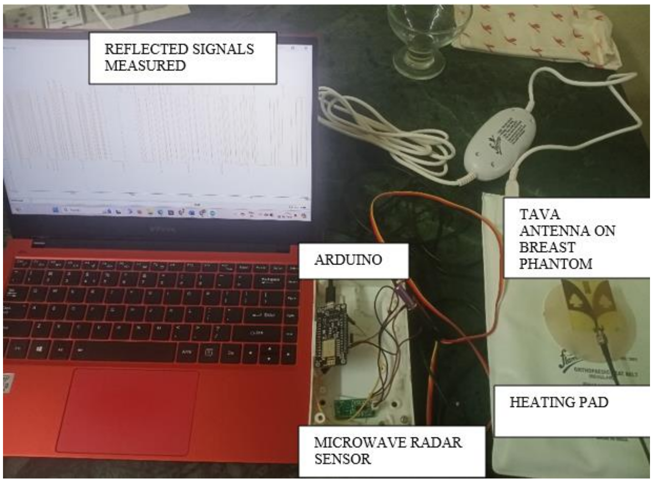

(b) Experimental set up using ABCD

Figure 8. Proposed ABCD device

3.5 Experimental analysis of proposed PBCD device

In passive sensing-based cancer cell detection, the antenna absorbs radiation from cancer cells. TAVA antenna acts as a sensor and acquires radiation from the cancer cells. The radiation signal from the cancer cell is acquired using SigView software via a DAQ card. The signal acquired is shown in Figure 9. The signals are obtained by placing the antenna at different positions from the breast phantom with and without cancer cells. The acquired signals are further analyzed using MATLAB.

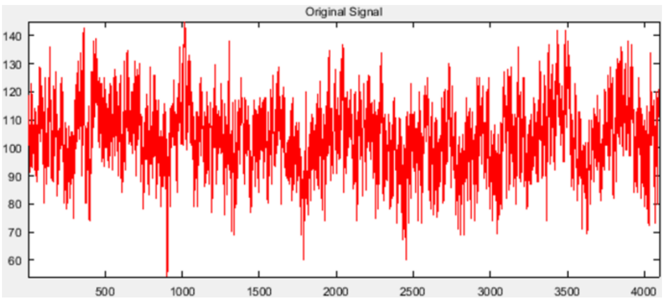

Figure 9. Radiated Signals from 3 mm cancer cells acquired using SigView software

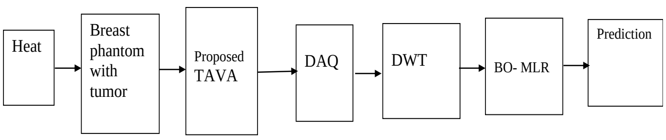

(a) Block diagram of PBCD

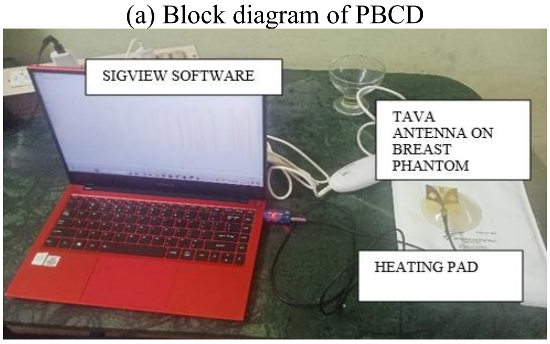

(b) Experimental set up using PBCD

Figure 10. Proposed PBCD device

In the PBCD, the radiated signal from the cancer cells acquired through the proposed TAVA is processed using the SigView software, which is shown in Figure 10(a) and Figure 10(b). The radiated signals are acquired from the breast without tumors and with tumors of different sizes. The antenna is placed in various locations, and the strength of the phantom signal is measured. From signal acquisition, the signal strength is maximum when the antenna is kept near the cancer cells.

The acquired signal is processed using a discrete wavelet transform. Discrete Wavelet Transform (DWT) preprocesses the signal and extracts the signal's features such as mean, standard deviation, median and variance. Figure 11 shows the histogram of the synthesized signal.

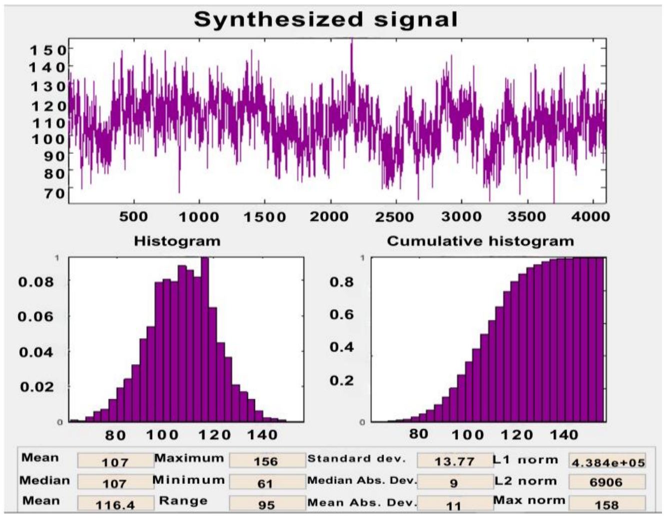

Figure 11. Features extracted using discrete wavelet transform for 3 mm cancer cell signal

The DWT is defined as:

$$W_{\emptyset}(j_0,k) = \frac{1}{\sqrt{M}}\sum_x f(x)\emptyset_{j0.k}(x) \tag{1}$$

$$W_{\varphi}(j,k) = \frac{1}{\sqrt{M}}\sum_x f(x)\,\varphi_{j.k}(x) \tag{2}$$

For $j>j_0$

Inverse DWT is defined as:

$$f(x) = \frac{1}{\sqrt{M}} \sum_x W_\emptyset(j_0, k) \emptyset_{j0.k}(x) + \frac{1}{\sqrt{M}} \sum_{j-j0}^{\infty} \sum_k W_\emptyset(j,k) \emptyset_{j,k}(x) \tag{3}$$

where, $f(x)$, $\emptyset(x)$ are functions of discrete variable.

From Table 6, the mean and median values are lower for signal without cancer cells and higher for cancer cells of size 5 mm and 3 mm. Similar readings were taken from different angle for the prediction of cancer size.

3.6 ML approach on cancer size prediction

The data are acquired for different cancer cells from ABCD and PBCD devices and are shown in Tables 6 and 7. The data are processed using the Bayesian optimization method. The cancer size is predicted using the machine learning algorithm. This paper proposes cancer size prediction using Bayesian optimized and multiple linear regression. *Linear regression* is a statistical technique that analyses the relationship between a dependent variable and one or more independent variables. Linear regression is limited to one independent variable, while multiple linear regression includes two or more independent variables.

Table 6. Features of discrete wavelet transform

No.	Size of the Antenna	Location	Mean	Sum	Median	Std Dev	Variance
1	No Tumor	Subcutaneous Region	66.59	272758	67	13.02	169.7
2	5mm Tumor	Subcutaneous Region	118.93	487178	119	13.41	179.88
3	3mm Tumor	Subcutaneous Region	85.84	351629	86	12.485	155.88

Table 7. Evaluation measures of cancer size prediction using active antenna as sensor

Antenna Position from Skin Surface	Actual Size in mm	S11	Predicted Size	Accuracy
At surface	3	-26.47	3.23456	92.181
1 cm	3	-26.12	3.07776	97.408
1.5 cm	3	-25.99	3.01952	99.349
2 cm	3	-25.94	2.99712	99.904
At surface	4	-29.54	4.60992	84.752
1 cm	4	-28.03	3.93344	98.336
1.5 cm	4	-27.87	3.86176	96.544
2 cm	4	-27.13	3.53024	88.256
At surface	5	-30.23	4.91904	98.381
1 cm	5	-30.34	4.96832	99.366
1.5 cm	5	-30.13	4.87424	97.484
2 cm	5	-30.04	4.83392	96.678

The R-squared method is used to assess the model's performance.

In linear regression, the equation is as follows:

$$y = \beta_0 + \beta_1 x \tag{4}$$

where, y is the dependent variable and x is the independent variable.

Bayesian optimized regression is a preferable alternative when the assumptions of linear regression, such as normality of data and linearity of predictor variables, are not met. This method integrates prior knowledge or beliefs about the data, leading to better understanding and accuracy in predictions. Bayesian optimization is beneficial for complex or unclear datasets, as it considers the uncertainty of refined estimates. This method is based on Bayes, given the observed data.

3.6.1 BO-linear regression – ABCD devices

In this measurement, cancer size is the dependent variable, and the SAR coefficients obtained from the phantom with an active TAVA antenna as the sensor are the independent variables.

Bayesian optimization seeks to identify the most accurate values for the parameters that define a linear model, which captures the underlying connection between predictor variables and a response variable. This linear relationship can be mathematically expressed as a function of the dependent variable Y and the independent feature set X, as follows:

$$Y = f(x, w) + \varepsilon \tag{5}$$

The regression coefficients w represent the connections between the independent variables and the dependent variable. These errors, ε, are independent and follow a normal distribution with a mean of 0 and a variance of σ^2.

Given the predictors x, target Y follows a normal distribution with mean $\mu = f(x,w) = w_0 + w_1x_1 + w_2x_2 + \ldots + w_px_p$ and variance σ^2.

The conditional probability density function (PDF) of Y given the predictor variables is shown in Eq. (6).

$$P(y|x, w, \sigma^2) = \frac{1}{\sqrt{2\pi\sigma^2}} e^{-\frac{(y-f(x,w))^2}{2\sigma^2}} \tag{6}$$

Eq. (7) shows the ABCD device predictor equation:

$$\text{Cancer size} = 0.448 \times \text{SAR} - 8.624 \tag{7}$$

From the analysis, Correlation, r= 0.953.
R- squared, $r^2 = 0.909$.

Table 7 shows the accuracy of the predicted cancer cell size with the actual cancer cell size. It is observed that cancer cells can be predicted with TAVA up to a distance of 2 cm from the skin surface. For a 3 mm tumor the machine learning algorithm has predicted the cancer cell size as 2.99.

3.6.2 BO-multiple regression approach on PBCD and prediction of cancer cell

In this approach, cancer size is the dependent variable and the mean value obtained after performing discrete wavelet transform is the independent variable.

$$\text{Cancer size} = 0.234 \times \text{mean value of the DWT} - 22.1655 \tag{8}$$

From the analysis, Correlation, r= 0.9618.

R- squared, $r^2 = 0.925$.

In cancer size prediction, multiple linear regression is optimized with Bayesian optimization (BO).

The BO- multiple linear regression for PBCD is as given below:

$$y = \beta_0 + \beta_1 x_1 + \beta_2 x_2 + \beta_{1,1} x_1 \times x_1 + \beta_{1,2} x_1 \times x_2 + \beta_{2,2} x_2 \times x_2 \tag{9}$$

Cancer size is predicted using the following equation:

$$\text{Cancer size} = 34.345 - 1.4591\ \text{mean} + 5.564\ \text{standard deviation} + 0.0063\ \text{mean} \times \text{mean} + 0.0164\ \text{mean} \times \text{standard deviation} - 0.2518.\ \text{standard deviation} \times \text{standard deviation} \tag{10}$$

Overall fit is given by R – squared, $r^2 = 0.9965$

Table 8 shows the evaluation measures for predicting the cancer cell size. It is observed that prediction of the cancer size is more accurate for BO multiple linear regression than BO linear regression. Cancer size of 3 mm can be predicted using this approach.

Table 8. Evaluation measures of cancer size prediction using regression analysis

Antenna Position from Skin Surface	Actual Size in mm	Mean	Std Deviation	BO Linear Regression		BO Multiple Linear Regression	
				Predicted Size	Accuracy	Predicted Size	Accuracy
at surface	5	120.12	12.49	5.94	81.15	4.79	95.21
1 cm	5	118.19	13.24	5.49	90.18	5.09	94.91
1.5 cm	5	115.8	13.39	4.93	98.63	4.65	95.35
2 cm	5	114.85	13.34	4.71	94.19	4.41	95.59
at surface	10	133.91	12.50	9.17	91.69	9.59	90.41
1 cm	10	132.26	13.07	8.78	87.83	9.63	90.37
1.5 cm	10	131.35	13.5	8.57	85.70	9.68	90.31
at surface	3	106.46	12.77	2.75	91.54	2.69	97.30
1 cm	3	103	13.41	1.94	77.46	2.87	97.12
1.5 cm	3	101.55	13.46	1.59	63.89	2.83	97.17

4. CONCLUSIONS

Table 9. Performance of proposed method

Method	Cancer Cell	Accuracy %
ABCD	3MM TUMOR	99.90%
PBCD	3MM TUMOR	97.30%

A novel TAVA has been developed on an FR-4 substrate, measuring 53.07 × 46.07 × 0.6 mm^3. TAVA has been utilized for cancer cell detection in a breast phantom model, mimicking human breast properties. The design of AVA has been finalized based on the accuracy in SAR analysis measured using the simulation software. Through SAR analysis, it is evident that the proposed TAVA antenna is able to detect single and multiple tumors of size 3mm placed at the lobules. Maximum radiation is obtained at the regions near tumor. These simulation results are validated in the real time conditions through ABCD and PBCD. Using active sensing method reflection coefficients are measured with and without tumor and observed a significant deviation in the reflection coefficients. Tumors of various sizes (3 mm, 4 mm, and 5 mm) have been successfully located using the proposed ABCD and PBCD methods. The study demonstrated a clear concentration of radiation in the tumor regions, with accurate detection of single and multiple tumors due to the inducing of heat. The analysis of reflected signals showcased significant differences between signals with and without cancer cells, effectively detecting cancer cells sized 3mm. Finally, bayesian optimized simple and multiple linear regression algorithms are applied to the statistical values to predict the cancer cell size. Using the proposed TAVA antenna, it is possible to predict cancer cells with a size of less than 3 mm when compared to the traditional antenna as a sensor with an accuracy of 99%. Table 9 shows the performance accuracy of the proposed method.

5. FUTURE RECOMMENDATIONS

The proposed system gave the best results for tumors present in subcutaneous region. But the tumors present in intercoastal muscle region were not able to detect accurately. The proposed devices can be updated with a Digital signal processor to detect cancer cell sizes below 2mm to 1mm, and generative artificial intelligence signals can be used to detect cancer cells.

ACKNOWLEDGEMENT

I thank Dr. N R Shanker and Physician Dr. R Aarthe for their valuable support of experimental result verification.

REFERENCES

[1] Borja, B., Tirado-Mendez, J.A., Jardon-Aguilar, H. (2018). An overview of UWB antennas for microwave imaging systems for cancer detection purposes. Progress In Electromagnetics Research B, 80: 173-198. https://doi.org/10.2528/PIERB18030302

[2] Aydin, E.A. (2018). Evaluation of breast tumor with Antipodal Vivaldi Antenna. Majlesi Journal of Telecommunication Devices, 7(1): 1.

[3] Kibria, S., Samsuzzaman, M., Islam, M.T., Mahmud,

M.Z., Misran, N., Islam, M.T. (2019). Breast phantom imaging using iteratively corrected coherence factor delay and sum. IEEE Access, 7: 40822-40832. https://doi.org/10.1109/ACCESS.2019.2906566

[4] Bhargava, D., Rattanadecho, P. (2022). Microwave imaging of breast cancer: Simulation analysis of SAR and temperature in tumors for different age and type. Case Studies in Thermal Engineering, 31: 101843. https://doi.org/10.1016/j.csite.2022.101843

[5] Kaur, G., Kaur, A. (2020). Breast tissue tumor detection using "S" parameter analysis with an UWB stacked aperture coupled microstrip patch antenna having a "+" shaped defected ground structure. International Journal of Microwave and Wireless Technologies, 12(7): 635-651. https://doi.org/10.1017/S1759078719001442

[6] Palantei, E., Amir, A., Dewiani, I.S.A., Achmad, A. (2015). Early stage cancer detection technique considering the reflected power from breast tissues. ARPN Journal of Engineering and Applied Sciences, 10(17): 7361-7367.

[7] Rajput, J.L., Nandgaonkar, A.B., Nalbalwar, S.L., Wagh, A.E., Huilgol, N.G. (2021). Performance evaluation of compact rectangular microstrip antenna for breast hyperthermia. International Journal on "Technical and Physical Problems of Engineering", 13(48): 87-94.

[8] Islam, M.T., Islam, M.T., Samsuzzaman, M., Arshad, H., Rmili, H. (2020). Metamaterial loaded nine high gain vivaldi antennas array for microwave breast imaging application. IEEE Access, 8: 227678-227689. https://doi.org/10.1109/ACCESS.2020.3045458

[9] Islam, M.T., Mahmud, M.Z., Misran, N., Takada, J.I., Cho, M. (2017). Microwave breast phantom measurement system with compact side slotted directional antenna. IEEE Access, 5: 5321-5330. https://doi.org/10.1109/ACCESS.2017.2690671

[10] Dixit, A.S., Kumar, S. (2020). A survey of performance enhancement techniques of Antipodal Vivaldi Antenna. IEEE Access, 8: 45774-45796. https://doi.org/10.1109/ACCESS.2020.2977167

[11] Balaji, A., Karthi, J., Chinnammal, V., Malarvizhi, C., Vanaja, S. (2021). A unique technique to improve the performance of Antipodal Vivaldi Antenna for microwave imaging application. IOP Conference Series: Materials Science and Engineering, 1055(1): 012100. https://doi.org/10.1088/1757-899X/1055/1/012100

[12] Hasim, N.S.B., Ping, K.A.H., Islam, M.T., Mahmud, M.Z., Sahrani, S., Mat, D.A.A., Zaidel, D.N.A. (2019). A slotted UWB Antipodal Vivaldi Antenna for microwave imaging applications. Progress in Electromagnetics Research M, 80: 35-43. https://doi.org/10.2528/PIERM18121201

[13] Amiri, M., Tofigh, F., Ghafoorzadeh-Yazdi, A., Abolhasan, M. (2017). Exponential Antipodal Vivaldi Antenna with exponential dielectric lens. IEEE Antennas and Wireless Propagation Letters, 16: 1792-1795. https://doi.org/10.1109/LAWP.2017.2679125

[14] Teni, G., Zhang, N., Qiu, J., Zhang, P. (2013). Research on a novel miniaturized Antipodal Vivaldi Antenna with improved radiation. IEEE Antennas and Wireless Propagation Letters, 12: 417-420. https://doi.org/10.1109/LAWP.2013.2253592

[15] Herzi, R., Bouslama, M., Gharsallah, A. (2017). Enhanced radiation characteristics for Antipodal Vivaldi Antenna using high permittivity dielectric director. Journal of Advanced Dielectrics, 7(3): 1750018. https://doi.org/10.1142/S2010135X17500187

[16] Abbosh, A.M., Kan, H.K., Bialkowski, M.E. (2006). Design of compact directive ultra wideband antipodal antenna. Microwave and Optical Technology Letters, 48(12): 2448-2450. https://doi.org/10.1002/mop.21955

[17] Shi, X., Cao, Y., Hu, Y., Luo, X., Yang, H., Ye, L.H. (2021). A high-gain Antipodal Vivaldi Antenna with director and metamaterial at 1–28 GHz. IEEE Antennas and Wireless Propagation Letters, 20(12): 2432-2436. https://doi.org/10.1109/LAWP.2021.3114061

[18] De Oliveira, A.M., de Oliveira Neto, A.M., Perotoni, M.B., Nurhayati, N., Baudrand, H., de Carvalho, A., Justo, J.F. (2021). A fern Antipodal Vivaldi Antenna for near-field microwave imaging medical applications. IEEE Transactions on Antennas and Propagation, 69(12): 8816-8829. https://doi.org/10.1109/TAP.2021.3096942

[19] Honari, M.M., Ghaffarian, M.S., Mirzavand, R. (2021). Miniaturized Antipodal Vivaldi Antenna with improved bandwidth using exponential strip arms. Electronics, 10(1): 83. https://doi.org/10.3390/electronics10010083

[20] Dvorsky, M., Ganesh, H.S., Prabhu, S.S. (2019). Design and validation of an Antipodal Vivaldi Antenna with additional slots. International Journal of Antennas and Propagation, 2019(1): 7472186. https://doi.org/10.1155/2019/7472186

[21] Dey, U., Singhal, A. (2014). Design of Antipodal Vivaldi Antenna in matching medium for microwave medical imaging. International Journal of Engineering Research & Technology, 3(10): 1236-1239.

[22] Islam, M.T., Samsuzzaman, M., Kibria, S., Islam, M.T. (2018). Experimental breast phantoms for estimation of breast tumor using microwave imaging systems. IEEE Access, 6: 78587-78597. https://doi.org/10.1109/ACCESS.2018.2885087

[23] Patel, P., Raina, A. (2021). Comparison of machine learning algorithms for tumor detection in breast microwave imaging. In 2021 11th International Conference on Cloud Computing, Data Science & Engineering (Confluence), Noida, India, pp. 882-886. https://doi.org/10.1109/Confluence51648.2021.9377191

[24] Sami, H., Sagheer, M., Riaz, K., Mehmood, M.Q., Zubair, M. (2021). Machine learning-based approaches for breast cancer detection in microwave imaging. In 2021 IEEE USNC-URSI Radio Science Meeting (Joint with AP-S Symposium), Singapore, pp. 72-73. https://doi.org/10.23919/USNC-URSI51813.2021.9703518

[25] Papini, L., Badia, M., Sani, L., Rana, S.P., et al. (2023). Breast cancer detection using machine learning approaches on microwave-based data. In 2023 17th European Conference on Antennas and Propagation (EuCAP), Florence, Italy, pp. 1-5. https://doi.org/10.23919/EuCAP57121.2023.10133340

[26] Tissue Frequency Chart. https://itis.swiss/virtual-population/tissue-properties/database/tissue-frequency-chart/.